Available online at www.sciencedirect.com
ScienceDirect
Trans. Nonferrous Met. Soc. China 35(2025) 3836−3851
Transactions of Nonferrous Metals Society of China
www.tnmsc.cn

Impact of γ- and β-radiation on metal-based tunneling junction devices and their restorability

Zhong-zheng TIAN, Da-cheng YU, Zhong-yang REN, Jiao-jiao TIAN, Li-ming REN, Yun-yi FU

School of Integrated Circuits, Peking University, Beijing 100871, China

Received 1 March 2024; accepted 15 May 2024

Abstract: Nanoscale metal-based tunneling junction (MTJ) devices were fabricated using the electromigration method, and their electrical properties were studied after exposure to γ- and β-radiation. Irradiation caused the set threshold voltage (V_{set}) of the MTJ devices to increase, leading to a transition from a low-resistance state (LRS) to a high-resistance state (HRS). This shift in V_{set} was due to atom displacement from high-energy electrons excited by γ- and β-radiation. Unlike semiconductor devices, MTJ devices showed resilience to permanent damage and could be restored in-situ through multiple I−V (I is the drain current; V is the drain voltage) sweeps with appropriate configurations. This ability to recover suggests that MTJ devices have promising potential under irradiation. The reparability of irradiated MTJ devices is closely related to nothing-on-insulator (NOI) their structure, providing insights for other NOI and metal-based micro-nanoscale devices.

Key words: γ-radiation; β-radiation; nanogap; metal-based tunneling junction; radiation damage

1 Introduction

Semiconductor devices are vulnerable to long-term radiation effects from high-energy particles such as photons and electrons [1−3]. This radiation can cause defects in the device channel, including dislocations, bond breakage, and the formation of interstitial atoms, which reduce carrier mobility [2−4]. Additionally, trapped charges and defects in the gate dielectric can lower breakdown voltages, increase leakage current, shift threshold voltage, reduce transconductance, and raise power consumption [1,5,6]. These combined effects are known as total ionizing dose (TID) effects [7,8]. Silicon or III−V compound devices can partially repair radiation damage through techniques like high-temperature annealing, but they lack the ability for on-chip, in-situ repair, thus limiting their performance in irradiated environments. Consequently, irradiation can irreversibly degrade device performance, making them unreliable in high-radiation conditions without expensive shielding or specialized fabrication processes such as fully-depleted silicon-on-insulator (FD-SOI) [9,10].

In recent years, metal-based tunneling junction (MTJ) switching devices have gained significant attention due to their small size, low power consumption, high speed, and ability to withstand high temperatures (up to 850 K) [11−13]. These devices show great potential for use in memory, logic, and synaptic applications. MTJs operate by utilizing atomic migration on electrode surfaces to adjust tunneling distances, enabling switching behavior [14].

Nanoscale MTJ devices exhibit unique radiation resistance due to their distinct materials and structures compared to traditional semiconductor

Corresponding author: Yun-yi FU, E-mail: yyfu@pku.edu.cn
https://doi.org/10.1016/S1003-6326(25)66916-0

devices. The use of inert precious metals like Au and Pd in MTJs contributes to their remarkable properties. At the nanoscale, these metals not only display exceptional catalytic activity [15,16], but also serve as stable, reliable electrodes, enabling high integration densities [12,17]. The high electron density in these metals (10^{22}−10^{23}/cm^3) [18,19] makes MTJ devices less prone to radiolytic damage than semiconductor materials [20−24].

Structurally, MTJs resemble a nothing-on-insulator (NOI) configuration [25−29], with a vacuum- or air-based tunneling barrier between the electrodes, eliminating the need for a dielectric, solid-state electrolyte, or semiconductor medium [30−32]. This design avoids conductive filaments, unlike memristor devices, enabling direct electron tunneling without channel materials. As a result, radiation-induced defects common in semiconductors, such as increased defect concentration and reduced breakdown voltage, are absent in MTJ devices, making them theoretically more radiation-resistant.

Recent studies, such as those by FAN et al [29], have highlighted the radiation resistance of nanoscale air channel devices (NACDs). However, to date, no reports have focused on the radiation resistance of nanoscale tunnel junctions. In this study, we investigated the effects of γ- and β-ray irradiation on nanoscale MTJ devices fabricated via the electromigration method. The results show that radiation primarily increases the set threshold voltage (V_{set}) and shifts the devices from a low-resistance state (LRS) to a high-resistance state (HRS). The impact varies depending on the metal material, and Pd-based devices generally exhibit less change than Au-based ones.

Unlike semiconductor devices, MTJ devices do not suffer structural degradation under γ- and β-ray irradiation. While irradiation affects the V_{set}, the material integrity remains intact. Pd- and Au-based MTJ devices can be restored to their original state through in-situ, on-chip electrical operations, without requiring additional processes like annealing. This repairability is an important feature of the radiation resistance inherent in NOI structures and may extend to other similar devices. These findings highlight the potential and challenges of deploying MTJ devices in high-radiation environments, such as space stations, satellites, reactors, and synchrotron radiation sources [22].

2 Experimental

2.1 Preparation of MTJs

The MTJ devices in this study were fabricated using a combination of electromigration and nanofabrication techniques. Firstly, metal nanowires, serving as the conductive channel, were created using the electron beam lithography (EBL), metal deposition, and lift-off technique. The nanowires are shaped into a neck configuration, with the narrowest point being 100 nm. A schematic of the metal nanowire device and its electrical test structure is shown in Fig. 1(a). For Au- or Pd-based tunneling junctions, the metal nanowires are made from a single metal (Au or Pd), with no adhesive metal layer. However, a Ti layer (0.3 nm) was first applied, followed by a Pd layer (5 nm), which served as an adhesive for the contact pads before depositing a 75 nm Au layer. The 5 nm Pd layer also prevented Ti oxidation and enhanced the structural strength of the electrode plate, ensuring reliability during electrical testing. The MTJ device was fabricated on a SiO_2/Si substrate, with a 300 nm SiO_2 layer covering the Si surface. The Si substrate was n-type doped with a low resistivity less than 0.2 Ω·cm. EBL was performed using a Voyager system from Raith, with an acceleration voltage of 50 kV and a standard exposure dose of 780 μC/cm². Metal deposition was carried out with the DE200 electron beam deposition system from Deyi Technology Co., Ltd., China, under a vacuum of 1.33×10^{-4} to 1.33×10^{-6} Pa and a deposition rate of 0.5 Å/s.

Subsequently, the metal nanowire was electromigrated and disconnected by I−V (I is the drain current; V is the drain voltage) sweep to form a tunneling junction device with nanoscale gap. Figure 1(a) displays an atomic force microscope (AFM) image of a gold tunneling junction device, with the nanogap indicated by the arrow. The inset in Fig. 1(a) shows an illustration of the gold nanowire device and its associated electrical test structure. Figure 1(b) presents a high-resolution transmission electron microscopy (HRTEM) image of a typical Au-based tunneling junction device, with a gap size of about 13 nm. Scanning electron microscopy (SEM) and AFM images of the Pd-based devices can be found in Fig. S1 in Supplementary Materials (SM). Different tunneling

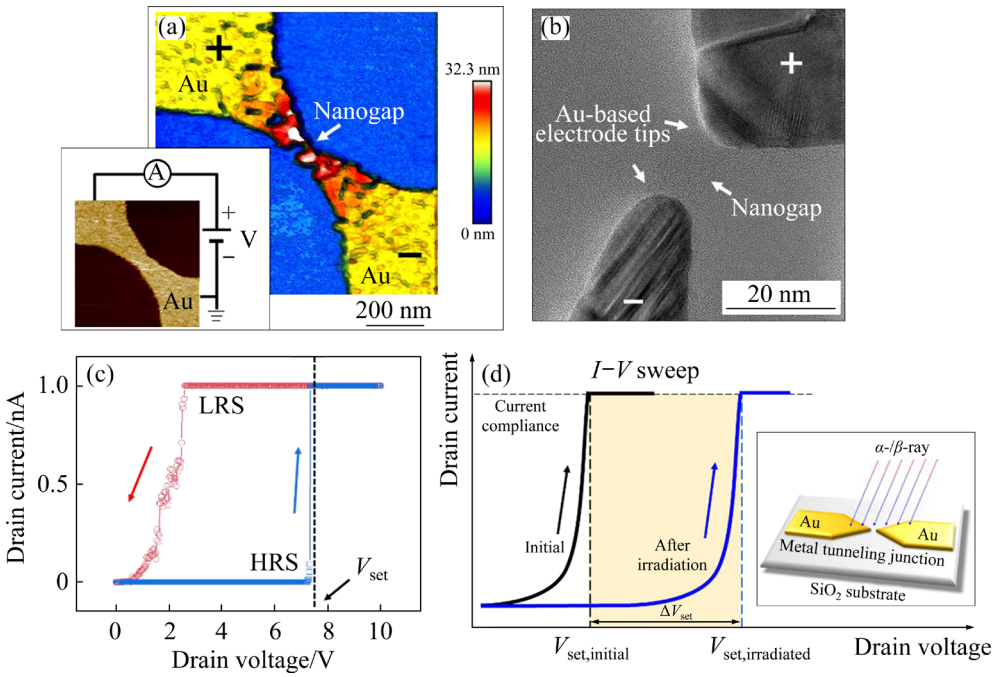

Fig. 1 MTJ and its electrical characteristic curves: (a) AFM morphology; (b) HRTEM image; (c) Hysteresis curves; (d) Schematic diagram illustrating I−V curves of metal nano gap junction before and after γ- or β-radiation (Inset: illustration of radiated MTJ device)

junction devices fabricated by electromigration have different gap sizes, which are distributed in the range of 1.1−20 nm. The radius of curvature of the electrode tips on both sides of the gap is 1−5 nm.

Electromigration is a commonly used method to prepare MTJs [17,33]. The test equipment for electromigration and electrical properties in this work was a Keysight B1500A semiconductor parameter analyzer and an MPIS T−150 probe platform, and the tests were carried out at room temperature and in atmospheric environment. The specific preparation process is as follows: Firstly, the voltage is applied on the metal nanowires in the single I−V sweep mode, that is, the drain voltage ramps from zero to a certain voltage (e.g., 3 V) at a constant speed of 0.5 V/s. Initially, the current increases linearly with the increase of the voltage, until to a threshold of 0.5−5 mA in the drain voltage of 0.2−2.5 V. At this time, due to the minimum cross-sectional area and the highest current density in the neck of nanowires, intense electromigration occurred under the combined action of "electronic wind" force and Joule heat [34,35]. The neck broke rapidly and formed a nano gap, and the drain current dropped from milliamperes to microamperes (Figs. S2(a) and (b) in SM). Subsequently, multiple I−V sweeps eventually reduced the drain current of the nanowires to the nanoampere level (Fig. S2(c) in SM). Finally, a current compliance (e.g., 1 nA) was applied to protecting the device, followed by bidirectional I−V sweep where the voltage increased to the maximum (e.g., 20 V) and then decreased to zero. A current hysteresis window (Fig. 1(c)) observed during this double-sweep confirmed the successful fabrication of the MTJ, with the tunneling junction switching from a high resistance state (HRS) to a low resistance state (LRS) after the hysteresis. The drain voltage during increasing phase, at which the current reached the compliance, was defined as the threshold voltage of SET operation, i.e., V_{set} of this device for its resistance state (Fig. 1(c)).

In this investigation, alongside the Au-based tunneling junction device, the electromigration technique was employed to fabricate the Pd MTJ device. Through the electromigration process, the Au- and Pd-based nanowires undergo gradual disconnection, resulting in a similar evolution trend of the I−V curves during the formation of MTJ devices. The main difference lies in the threshold voltage for the breakdown of Au- and Pd-based

nanowires during the I−V sweep. The threshold voltage of Au-based nanowire fracture ranges between 0.3 and 1.1 V (average 0.61 V), while for Pd-based nanowire fracture, it ranges between 0.7 and 1.6 V (average 0.91 V), as depicted in Fig. S3 in SM.

2.2 Impact of γ- or β-radiation on MTJ devices

For γ-radiation experiments, a ^{60}Co source emitting photons with energies of 1.333 and 1.173 MeV was utilized [36]. The radiation setup included a complete system with a console, a irradiation chamber, and a dose monitoring equipment. Device samples were enclosed in a plastic tube and placed in the cobalt source chamber, where they were irradiated with γ-rays in an atmospheric environment. The radiation dose rate was set to 203.3 rad/s, and the radiation dose was controlled by adjusting the radiation time. Three radiation doses were applied: 0.1, 0.5, and 1 Mrad to study the impact of γ-rays on the MTJ devices.

β-ray radiation was carried out under a scanning electron microscope (SEM). Since β-radiation essentially involved a high-speed electron flow, the electron beam in SEM was utilized to simulate the β-radiation from radioisotopes ^{63}Ni and evaluate its impact on the semiconductor devices [21,23,37−41]. The SEM used for β-ray (or electron beam) irradiation was an FEI strata DB235 SEM-FIB dual beam system and an FEI Nova nano 430 SEM system. The acceleration voltage was 15 and 30 kV, and the total dose was 20, 100 and 200 C/cm^2, respectively. β-radiation was performed under vacuum conditions (<1.33×10^{-4} Pa) at room temperature.

To assess the impact of γ- and β-radiation on the MTJ devices, the set voltage (V_{set}) and the change in V_{set} (ΔV_{set}) were used as key metrics. All electrical tests, whether before or after irradiation, were conducted under atmospheric conditions at room temperature. The experimental procedure is as follows.

(1) Initial measurement

The I−V curve of each tunneling junction device was measured in single I−V sweep mode using the probe stage and semiconductor parameter analyzer to establish a reference. The initial V_{set}, denoted as $V_{set\text{-}initial}$, was recorded for each device. All test parameters (e.g., voltage range, sweep rate, and current compliance) remained same for all devices. Each device was measured at least twice to ensure the stability of its I−V curve and the corresponding $V_{set\text{-}initial}$, confirming that these values do not change spontaneously.

(2) Irradiation

The devices were then placed either into the cobalt source chamber for γ-radiation at a specified dose rate, or into the SEM vacuum chamber for β-radiation. Once the device is accurately focused, the beam current and field of view will be recorded to calculate the irradiation dose rate. The total irradiation dose was controlled by adjusting the exposure time.

(3) Post-irradiation measurement

After irradiation, the I−V curves were measured again with the same parameters as initial tests. The V_{set} recorded at this stage was denoted as $V_{set\text{-}irradiated}$. The difference between the $V_{set\text{-}irradiated}$ and $V_{set\text{-}initial}$ values is calculated, and this change is referred to as ΔV_{set}, which is defined as

$$\Delta V_{set} = V_{set\text{-}irradiated} - V_{set\text{-}initial} \quad (1)$$

This procedure allows for a detailed comparison of the MTJ devices' electrical properties before and after exposure to γ- and β-radiation. The I−V curves from the radiation tests are shown in Fig. 1(d).

(4) Testing under various radiation doses

If the device was tested under multiple doses, Steps (2) and (3) were repeated for each dose. The I−V curves for all devices were measured at different radiation doses and compared with their initial I−V curves. Prior to each radiation exposure, multiple double I−V sweeps were performed on each device to ensure consistency in the $V_{set\text{-}initial}$ across tests.

The V_{set} and ΔV_{set} were used to evaluate the impact of radiation on the MTJ devices, as they serve as key indicators of the tunneling distance between the electrode tips. For a given current compliance, a smaller V_{set} corresponds to a higher tunneling current, indicating a shorter tunneling distance, while a larger V_{set} corresponds to a longer tunneling distance and lower tunneling current. A positive ΔV_{set} suggests that the device has shifted to a lower current state (i.e., higher tunneling resistance), meaning it has transitioned from a LRS to a HRS, implying an increase in the tunneling distance. Conversely, a negative ΔV_{set} indicates a shift in the opposite direction.

V_{set} is also a critical performance parameter for

MTJ devices, particularly in practical applications like nanogap memory devices [13,30,42]. Therefore, the change in V_{set} under radiation is a significant concern from both functional and application perspective.

In total, 28 Pd-based devices (16 for γ-rays and 12 for β-rays) were irradiated, and 39 Au-based devices (9 for γ-rays and 30 for β-rays) were irradiated, to evaluate the impact of radiation on the MTJ devices. The pre-irradiation measurement, irradiation with a specific dose, and the post-irradiation measurement were completed within the maximum periods of 4.5 h for Pd-based devices, and 3.5 h for Au-based devices, respectively. Additionally, the retention of several other Pd- and Au-based devices was also tested without radiation to exclude possibility that the ΔV_{set} was caused by any spontaneous change in the devices' resistance states, as shown in Fig. S4 in SM. Retention tests confirm that Pd-based devices exhibit stability for over 24 h, while Au-based devices retain stability for over 10.5 h. Therefore, the ΔV_{set} discussed in this paper is exclusively induced by the radiation.

It is noteworthy that the maximum dose of γ-radiation is limited to 1 Mrad to ensure that the entire test procedure is completed within the retention time. The complete test procedure for each sample, including the initial electrical test, transportation to the cobalt source chamber, sample loading and unloading, safety inspections, radiation processes, and the post-irradiation electrical test, must be completed within the retention time of 10.5 h. The only cobalt source available for this study provides a non-adjustable dose rate of 203.3 rad/s. Meaningfully, higher doses (e.g, 5 or 10 Mrad) will extend the test procedure beyond 10.5 h, potentially leading to spontaneous switching of the MTJ devices. While MTJ devices can certainly withstand much higher doses, the results will be less convincing if they cannot be distinguished from spontaneous resistance state switching. Additionally, 1 Mrad is an effective dosage endpoint for observing total dose effects in conventional semiconductor devices such as flash memory [7,8,43]. Therefore, 1 Mrad was selected as the dose endpoint for γ-radiation in this study.

3 Results and discussion

3.1 Impact of γ-radiation on Pd- and Au-based tunneling junction devices

Figure 2 shows the effect of γ-radiation on Pd- and Au-based tunneling junction devices. In each curve, the position of the V_{set} is labeled by a vertical dash reference line. The shape of the I–V curves for "SET" operation of MTJ devices did not show significant changes under γ-radiation. However, there was a notable rightward shift in the I–V curve, leading to an increase in $V_{set\text{-}irradiated}$ and inducing a positive ΔV_{set}. Figure 2(a) shows the test results of a typical Pd-based tunneling junction device. The device was irradiated with a single dose of 0.1, 0.5, and 1 Mrad of radiation, resulting in cumulative doses of the device were 0.1, 0.6, and 1.6 Mrad, respectively. As seen from Fig. 2(a), after three different doses of γ-radiation, the ΔV_{set} of the device

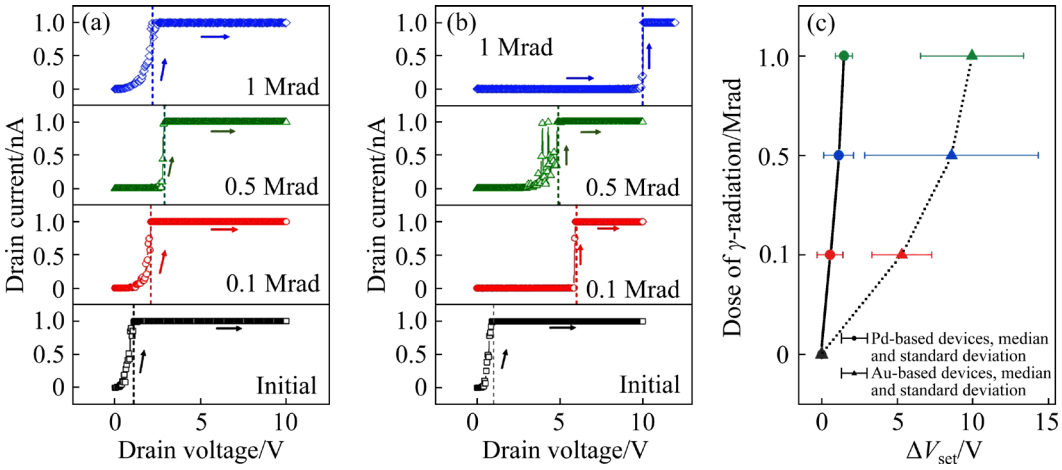

Fig. 2 Impact of γ-radiation on I–V curves of different MTJ devices: (a) Pd-based tunneling junction devices irradiated with different doses of γ-rays; (b) Au-based tunneling junction devices irradiated with different doses of γ-rays; (c) Statistical diagram of ΔV_{set} of irradiated Pd- and Au-based devices

is about 1.0, 1.9, and 1.2 V, respectively. Similarly, Fig. 2(b) shows a typical Au-based tunneling junction device after exposure to varying doses of γ-rays. After γ-radiation, the I–V curves also shifted significantly to the right. With a single dose of 0.1, 0.5 and 1.6 Mrad, and the cumulative dose of 0.1, 0.6 and 1 Mrad, the ΔV_{set} measured approximately 5.1, 3.9 and 9.1 V, respectively.

Figure 2(c) shows statistical data on ΔV_{set} for irradiated Pd- and Au-based devices. A positive correlation between the median ΔV_{set} and γ-ray dose is observed for both types of devices, although the relationship is not strictly linear. Over 200 I–V curves were collected from 16 Pd-based and 9 Au-based devices irradiated with varying doses of γ-rays. Nearly all ΔV_{set} values were positive, ranging from 0.5 to 15 V, with only 5 curves showing negative ΔV_{set} (<4 V in amplitude). These negative values have minimal impact on the overall statistics, reinforcing the positive correlation between ΔV_{set} and the radiation dose.

Furthermore, Au-based devices demonstrated significantly larger median ΔV_{set} compared to Pd-based devices at equivalent doses. At a dose of 1 Mrad, the maximum median ΔV_{set} for Au-based devices reached 10.0 V, nearly 7 times larger than that of Pd-based devices (1.5 V). On average, the median ΔV_{set} of Au-based devices was 8 times larger than that of Pd-based devices, suggesting a more substantial impact of cumulative γ-radiation on Au-based devices.

Both Pd-based and Au-based devices showed dispersion in ΔV_{set}, as indicated by the standard deviation bars, suggesting variability alongside the positive correlation observed at different doses. This is evident in the I–V curves of curves shown in Figs. 2(a) and (b). The Pd-based device exhibits a maximum ΔV_{set} of 1.9 V at 0.5 Mrad, but a smaller ΔV_{set} of 1.1 V at 1 Mrad. Similarly, the Au-based device shows a higher ΔV_{set} of 5.1 V at 0.1 Mrad compared to 3.9 V at 0.5 Mrad. Therefore, while a positive correlation between ΔV_{set} and dose is clear, a strict quantitative relationship cannot be established for individual MTJ device.

Seen from the I–V curves, all devices are found to function normally after being irradiated by γ-ray except for the shift of V_{set}. No permanent or fatal damage (e.g., breakdown or increased leakage current) was found, even at the highest dose of 1 Mrad.

3.2 Impact of β-radiation on Pd- and Au-based tunneling junction devices

Figure 3 illustrates the effect of β-radiation on Pd-based tunneling junction devices. In Figs. 3(a) and (b), the I–V curves of irradiated Pd-based devices shift to the right at various doses and accelerating voltages, indicating an increase in V_{set}. At 15 kV, the ΔV_{set} values are 3.7, 4.8, and 5.2 V at doses of 20, 100, and 200 C/cm², respectively. At 30 kV, the ΔV_{set} values are 2.2, 3.9 and 5.5 V at the same doses, respectively. The impact of β-rays (electron beam) on Au-based devices is shown in Fig. S5 in SM, also at voltages of 15 and 30 kV.

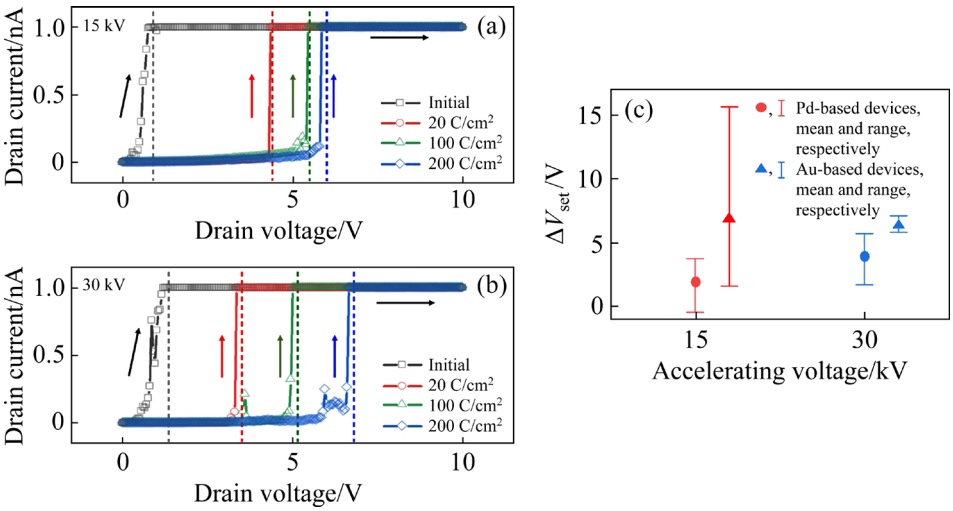

Fig. 3 Impact of β-rays (electron beams) on different MTJ devices: (a) Pd-based devices at 15 kV accelerating voltage; (b) Pd-based devices at 30 kV accelerating voltage; (c) Statistical data of ΔV_{set} of Pd- and Au-based devices irradiated by electron beams with dose of 100 C/cm²

Statistical analysis in Fig. 3(c) reveals that both Pd- and Au-based devices exhibit positive medium ΔV_{set} at both 15 and 30 kV and a dose of 100 C/cm^2. Pd-based devices show a smaller median ΔV_{set} compared to Au-based devices at both voltages, consistent with the results from γ-radiation experiments (Fig. 2(c)). However, Pd-based devices have a larger median ΔV_{set} at 30 kV than at 15 kV, while Au-based devices do not show this trend, indicating that the electron beam's accelerating voltage does not have a clear impact on ΔV_{set}. β-radiation (emulated by electron beams in this study) causes a shift from LRS to HRS in MTJ devices, with effects similar to those of γ-radiation. This is an intriguing result given the different natures of β-radiation (high-energy electrons) and γ-radiation (high-energy photons).

Just as γ-radiation, all devices are found to function normally after exposure to β-radiation, except for the shift of V_{set}. No permanent or fatal damage was observed across various doses and accelerating voltages.

3.3 Impact of cumulative γ- and β-radiation on MTJ devices

Experiments have revealed the following five crucial characteristics regarding the impact of the accumulative γ- and β-radiation on the Pd- and Au-based tunneling junction devices.

(1) All the irradiated devices exhibit an increased V_{set} (positive ΔV_{set}), indicating rightward shifts in their I−V curves.

(2) Only statistical analyses reveal a positive correlation between the median or mean of ΔV_{set} and the dose of irradiation, with no clear strict quantitative relation apparent in individual devices.

(3) Au-based devices generally have larger ΔV_{set} values than Pd-based devices in statistics analyses.

(4) Despite being irradiated at various doses and energies, all devices function normally except for the shifted V_{set}.

(5) Despite their different natures, γ- and β-radiation exhibits similar impact on V_{set} and ΔV_{set} of both Pd- and Au-based devices.

To understand the impact of accumulative γ- and β-radiation of the MTJ devices, a general theoretical framework is proposed. The framework is based on the theory of radiation damage in metal, and the physical switching mechanism of metal tunneling devices reveal that the impact arises from a combination of radiation-induced atom displacement/migration and the structure of the MTJ device, with high-energy electrons playing a pivotal role.

3.3.1 Generation of high-energy electrons

Both primary high-energy particles (such as photons in γ-rays and primary electrons in β-rays) and secondary particles (including secondary electrons, electron−positron pairs, and photons) are responsible for interacting with metal atoms. In the case of β-radiation (electron beam), the primary impact comes from the high-energy electron beam itself (Fig. 4(a)). In our experiments, the primary electron beam impacts the device at energies of 15 or 30 keV. For γ-radiation, the impact on metals primarily arises from high-energy secondary electrons generated by high-energy photons, rather than the photons themselves. This aligns with the radiation damage theory in metals [18,44−48].

Photons interact with atoms in four main ways: photoelectric absorption, Compton scattering, pair production, and photodisintegration. However, photodisintegration requires photon energy exceeding 10 MeV, which is beyond the energy range of γ-rays emitted by ^{60}Co (1.333 and 1.773 MeV) [36,47,49], and is therefore irrelevant to our experiments. Although pair production (with a threshold of 1.02 MeV) is possible, its cross-section is very small at the energies of ^{60}Co γ-rays (<0.1% of the total cross-section) [47]. So, it does not significantly contribute to the secondary electron generation. Thus, the main interactions in our study are Compton scattering and photoelectric absorption, both of which generate high-energy secondary electrons that contribute to radiation effects on the device, as shown in Fig. 4(b).

It is essential to clarify the terminology of secondary electrons (SEs) to avoid misunderstanding. In this work, secondary electrons encompass all electrons induced by inelastic collisions of radiation and atoms, including backscattering electrons (BSEs), Auger electrons and slow secondary electrons [50]. The slow secondary electrons, composed of electrons having energies of several tens of eV (typically in a SEM), are sometimes called as "secondary electrons" to differentiate from BSEs in some other literature [50]. The energy distribution of SEs changes from several eV to close to the energy of the primary particles [49,50].

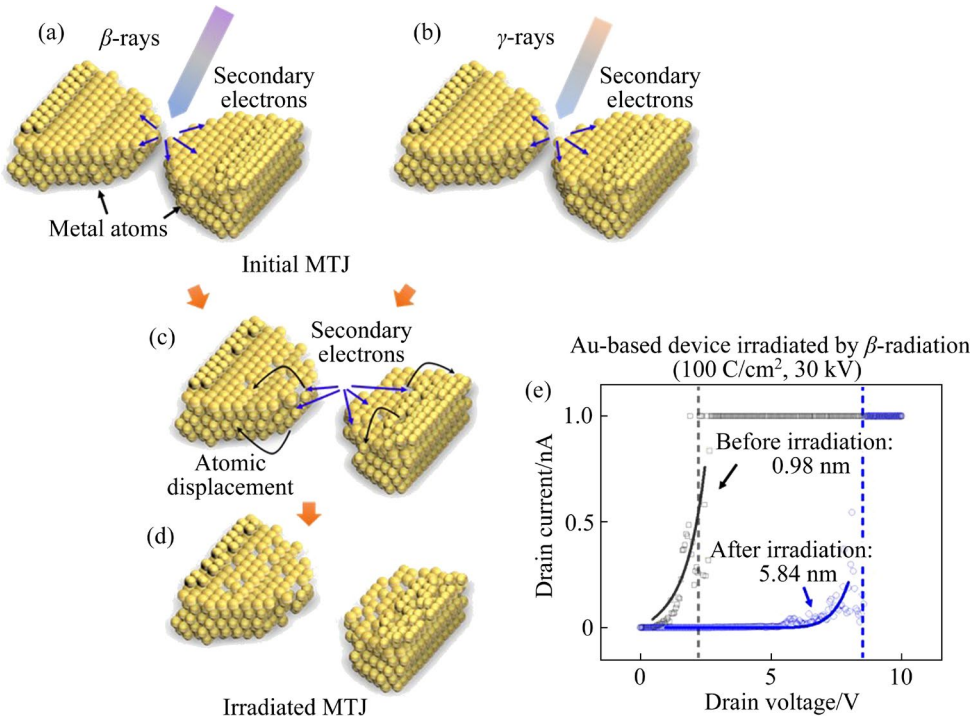

Fig. 4 Mechanism of β- and γ-radiation impact on tunneling distance of MTJ devices: (a, b) β- and γ-rays exciting high-energy electrons upon bombarding metal electrode tips, respectively; (c) High-energy SEs causing displacement of metal atoms moving away; (d) Tunneling distance increasing after irradiation; (e) Simmons formula fitting of I–V curves

In this work, the SEs can reach energies exceeding 1 MeV for γ-radiation (photon energy of ^{60}Co) through Compton scattering and photoelectric absorption [36,49,50], or 15 and 30 keV for β-radiation (electron beam) [50]. Additionally, SEs are abundant in quantity due to the cascade collision of each incident primary particle, leading to the creation of multiple SEs. The similarity in the impact of γ- and β-radiation on MTJ devices is readily inferred from the above analysis. Despite different natures of the radiated particles, high-energy electrons, either secondary electrons induced by photons of γ-radiation or primary electrons of the β-radiation (electron beam), are the main factor to cause atom displacements in metals. Thus, their impacts on the MTJ devices are natural.

3.3.2 Atom displacement and migration induced by high-energy electrons

The bombardment of metal atoms by high-energy SEs transfers kinetic energy to metal atoms through elastic collision in Coulomb interaction with the nuclei. When the maximum kinetic energy gained by a metal atom, E_{max}, exceeds its displacement energy, E_d, the atom will displace from the original lattice position in multiple ways to form knock-on damages, including forming interstitial atoms, sputtering and migration. Typically, E_d ranges from 10 to 50 eV for metals [18,19,44,45], comprising the energy required to form a pair of interstitial atom and vacancy. E_{max} is determined by conservation of energy and momentum, given by the relativistic formula [51]:

$$E_{max}=\frac{2ME_0(E_0+2mc^2)}{(m+M)^2c^2+2ME_0} \quad (2)$$

where M is the mass of the nucleus, c is the speed of light, m and E_0 are the mass and energy of the incident electron, respectively. Due to the huge difference in their mass, only a small fraction of the incident electron transfers to the atom. Hence, the E_0 should be in range of hundreds of keV to displace an atom. It seems that only the SEs generated by photons in γ-radiation can effectively displace metal atoms.

On the surface, however, the displaced atoms do not need to squeeze into an interstitial site, so the E_0 is much reduced. EGERTON et al [18,19] have suggested the use of the enthalpy of sublimation, E_s,

instead of E_d, to estimate E_0 in electron beam induced sputtering in TEM. Analogously, we suggest using migration energy E_m in MTJ devices to estimate the threshold energy for metal atoms to migrate on electrode tip surfaces. The metal atoms on the surface only need to migrate to any adjacent empty site on the surface to change the tunneling current, which will be discussed in the following section. The migration energies of Pd and Au atoms are calculated to be 1.19 and 0.83 eV, respectively [52]. Utilizing Formula (3), the upper limit for E_0 does not exceed 32 keV for both metals. Furthermore, recoil-enhanced atomic migration greatly reduces the migration energy in the direction of the electron beams [53]. Experiments have confirmed that, a 30 keV electron beam can cause considerable damage in Zr-alloy, whose E_0 values are calculated to be 433 and 210 keV for knock-on and sputtering, respectively [54]. Therefore, we propose that the β-radiation (15 and 30 keV) in this work is also sufficient to migrate Pd and Au atoms on the surface of the electrodes, similar to the SEs of the γ-radiation, as shown in Fig. 4(c).

3.3.3 Asymmetry change of tunneling distance in MTJ device

For an individual atom, the direction of displacement and migration caused by radiation is random. However, due to the tip structure in a MTJ device, radiation-induced atomic movement creates an asymmetry that increases the tunneling distance. An atom at the apex of the electrode's tip is considered, as shown in Fig. 4(d). Random migration in any direction typically shortens the electrode tip, increasing the tunneling distance. Atoms not at the apex can move in any direction, but only when an atom migrates toward the tip and eventually reaches the apex does it increase the tip size and decrease the tunneling distance. Clearly, the likelihood of increasing the tunneling distance is much higher than decreasing it, even with random atom displacements.

Higher radiation doses lead to more atomic displacements, causing a greater increase in the tunneling distance (on the nanometer scale), which results in lower tunneling current, and therefore, an increase in V_{set} and a positive ΔV_{set} (on the scale of several volts), as shown in Fig. 4(e).

Importantly, in the migration process on surfaces, metal atoms do not need to form interstitial atoms to displace. Atoms can migrate as long as they gain sufficient energy from collision with high-energy electrons. This migration energy is typically around 1 eV, which is 1/10−1/50 of the displacement energy [18,19,44,52,55,56]. This low migration energy facilitates the radiation-induced movement of atoms, particularly near the apex of the electrode tip.

The increased V_{set} and positive ΔV_{set} provide clear evidence of the increased tunneling distance between the metal electrode tips. The drain current of a MTJ device corresponds directly to the tunneling current through the vacuum or air gap, which forms the tunneling barrier between the metal electrode tips.

Generally, the tunneling current through a rectangular barrier under an applied bias voltage can be described using the Simmons formula. SIMMONS [57] proposed a universal tunneling current formula as an integral equation, which is too complex to fit experimental data. He later provided three distinct analytical approximations for low, intermediate, and high bias voltages, respectively. The applicability of these approximations is discussed in the SM.

In this study, the Simmons formula for the intermediate voltage range is used in the following form [57]:

$$I = A\left(\frac{e}{2\pi h d^2}\right)\left\{\left(\varphi-\frac{eV}{2}\right)\cdot \exp\left[-\frac{4\pi d}{h}(2m)^{1/2}\left(\varphi-\frac{eV}{2}\right)^{1/2}\right]- \left(\varphi+\frac{eV}{2}\right)\exp\left[-\frac{4\pi d}{h}(2m)^{1/2}\left(\varphi+\frac{eV}{2}\right)^{1/2}\right]\right\} \tag{3}$$

where A is the area, d is the tunneling distance, V is the applied bias voltage, e is the charge of electrons, h is the Planck constant, and φ is the barrier height (determined by the workfunction of the electrode metals). Formula (3) provides the best fitting of the tunneling current in the intermediate voltage range defined as $0<eV<\varphi$, which encompasses the primary working voltage of our MTJ devices. With a certain bias voltage, section area and barrier height, the tunneling current has a negative-exponent-like relation with the tunneling distance. A metal tunneling device with larger tunneling

distance (lower tunneling current) would have the I−V curve closer to the right side, resulting in a larger V_{set}. The increased tunneling distance can be estimated by fitting the I−V curves before and after irradiation of devices, as shown in Fig. 4(e). For example, the Au-based device has a $V_{set\text{-}initial}$ of 2.2 V before irradiation, and a $V_{set\text{-}irradiated}$ of 8.5 V after irradiated by electron beam (β-radiation) at the dose of 100 C/cm^2 and a accelerating voltage of 30 kV. The ΔV_{set} is 6.3 V. By fitting both I−V curves using Formula (3), the initial tunneling distance of the Au-based device was determined to be 0.98 nm. After irradiation, the tunneling distance increased to 5.84 nm, representing an increase of 4.86 nm. Similarly, the increased V_{set} and positive ΔV_{set} indicate that the tunneling distances of most of irradiated Pd- and Au-based devices increased compared to their initial ones.

The work functions of Pd (5.12 eV) and Au (5.10 eV) are very similar [58], yet the increase in V_{set} for Au-based tunnel junctions is typically larger than that for Pd-based junctions. This suggests that the increase in tunnel spacing in Au-based devices is more significant. The primary reason for this discrepancy is the lower migration energy of Au atoms (0.83 eV) compared to that of Pd atoms (1.19 eV) [52]. According to the theoretical framework of atom migration, the jump rate of an atom (f) is governed by the Arrhenius equation [52]:

$$f = f_0 \exp\left(-\frac{E_m}{k_B T}\right) \tag{4}$$

where f_0 is the attempting rate related to the thermal motion or kinetic energy of metal atoms, k_B is the Boltzmann constant, T is the temperature, and E_m is the migration energy. With migration energies of 1.19 eV for Pd and 0.83 eV for Au, Pd atoms are more difficult to displace than Au atoms, even when both are exposed to the same kinetic energy. Consequently, after irradiation, more Au atoms are displaced compared to Pd atoms, leading to a larger increase in the tunneling distance in Au-based devices. Thus, the impact of radiation on Au MTJ devices, as reflected by ΔV_{set}, is more pronounced than that on Pd MTJ devices.

While higher radiation doses increase the probability of more displaced atoms and a larger tunneling distance, this is not guaranteed for each individual device. The migration of atoms on the electrode surface is a random process, and the number of displaced atoms can vary with dose and from device to device. This variability explains why ΔV_{set} may be smaller at higher doses in certain devices (Figs. 2(a) and (b)). However, statistically, a positive correlation between ΔV_{set} and radiation dose is observed in the median and mean of ΔV_{set}, with randomness reflected in the standard deviation (Figs. 2(c) and 3(c)).

3.3.4 Effect of local temperature and electrical resistivity of metals

It is important to consider whether local temperature rises and changes in the metal's resistivity during irradiation could contribute to the observed changes in V_{set}. During the interaction between high-energy electrons and metal atoms, the kinetic energy is eventually dissipated as heat, leading to a local temperature rise. However, given the thin nature of the electrode layers in our devices (10 nm), most of the electrons penetrate the sample without dissipating significant heat inside the metal. Consequently, the local temperature increase due to radiation is only a few kelvins, which is unlikely to impact device performance significantly [18].

Defects in lattice induced by radiation are known to increase the electrical resistivity of metal [18,19]. However, the change of V_{set} in irradiated metal tunneling devices cannot be attributed to such mechanisms for three reasons: (1) The change of electrical resistivity of pure metal can only be accurately measured at low temperature (typically < 100 K). At room temperature, annealing would sufficiently eliminate most of the lattice defects, so that the resistivity change would be only several percents [18,44,45,48,55]. While in our devices, the change of tunneling current is caused by the changed tunneling distance, so that the resistivity change is over several orders of magnitude across different radiation doses, as evidenced by the I−V curves (Figs. 2(a), 2(b), 3(a) and 3(b)). (2) The change of resistivity in irradiated metals normally shows linear relationships with the dose [48]. While the statistics has shown no linear correlation between the dose and the ΔV_{set} (Fig. 2(c)) in our MTJ devices. (3) The measurement of electrical resistivity pertains to the conductive current of the metal, as resistance is governed by the Ohm's law. Although radiation may alter the conductive resistance, the change remains within the mΩ range due to their geometric dimensions in the case of our devices. Conversely, in a real MTJ device,

tunneling resistance ranges from GΩ (LRS) to TΩ (HRS) (Fig. 4(e)). The change in conductive resistivity is thus negligible compared to the tunneling resistance. In conclusion, the change of V_{set} must stem from the change of tunneling distance (and consequently tunneling resistance), rather than the change of electrical resistivity of metals.

The negligible change of electrical resistivity of metal also explains why all the devices remain functional after the irradiation. The electrode tips essential for forming a tunneling junction remain intact, with only slight changes in tunneling distance on the scale of several nanometers, and their conductivity remains unaffected by irradiation, ensuring that the tunneling current through the barrier of vacuum/air is undisturbed. This suggests the potential for in-situ repairability of the MTJ devices after irradiation.

3.4 In-situ repairability of irradiated MTJ devices

Building upon the analysis in the preceding section, we proposed a novel method for repairing MTJ devices affected by irradiation. The basis of this repairability lies in two key factors: (1) the nature of γ- and β-radiation damage on metal; (2) the NOI structure of the MTJ devices.

γ- and β-radiation, involving high-energy electrons, do not cause radiolytic damage in metals. Radiolytic damage typically occurs in low-conductivity materials, leading to broken bonds and lattice distortion [19,44]. Such damages in conventional semiconductor devices like MOSFETs lead to dangling bond, increased interface state, disordered channels, and reduced breakdown voltages. On the contrast, metal is protected from radiolytic damage due to its high electron density and excellent conductivity. Holes in the valence band excited by incident electrons can be refilled in less than 1 fs, much faster than the atomic vibration (100 fs), such that no change in the wavefunction of atomic electrons will be stimulated by the atomic vibrations, and interatomic bond remains. Therefore, knock-on damage is the only form of damage that occurs in irradiated metal, potentially changing the shape of the electrode tips in MTJ devices.

Additionally, the nanoscale geometry and the metal−vacuum−metal (MVM) structure of MTJ devices offer further protection. Like other NOI structures, MTJ devices lack dielectric or electrolyte layers, unlike RRAM devices, which may suffer permanent threshold shifts from radiation damage. MTJ devices are unaffected by such medium damage. Also, changes in conductivity of metal electrode tips are negligible compared to changes in tunneling resistance, as discussed earlier. The small size of MTJ devices ensures that only a small fraction of the radiation dose impacts the tunneling junctions, further reducing damage.

Consequently, it is concluded that MTJ devices irradiated with γ- and β-rays do not experience permanent or fatal damage. As long as the tunneling distance is restored, the devices can be repaired to their original state. Repair is achieved through in-situ electrical operations, specifically by applying multiple double I−V sweeps with optimized parameters like current compliance, ramping rate, and maximum voltage (Fig. 5). During the double I−V sweeps (Fig. 5(c)), electrostatic forces, electric field gradients, and the wind force of tunneling current drive atoms toward the electrode tip apex [34,59−61], gradually reducing the increased tunneling distance. While atoms may not return precisely to their original positions, the tunneling distance can be restored, and the I−V curve (representing resistance states) will closely match the original, as shown in Fig. 5(d). The recovery of the tunneling current indicates a successful repair, identifiable by V_{set}.

To efficiently drive atom migration, the repair process requires three conditions: (1) proper current compliance to ensure sufficient current without damaging the device; (2) a low ramping rate (<1 V/s) to allow enough time for atoms to migrate; (3) a maximum voltage higher than the irradiated V_{set} to create a strong electric field for driving atoms. These parameters can be adjusted for each device. Since MTJ devices remain functional after irradiation, the double I−V sweeps can be applied in-situ, as in previous tests. For example, as shown in Fig. 6(a), the Au-based device has an initial V_{set} of 5 V, which increases by 10 V after γ-radiation at 1 Mrad. After in-situ repair, V_{set} returns to the initial value. Figure 6(b) illustrates the repair process, with I−V sweep parameters of 1 nA current compliance, 0.25 V/s ramping rate, and 20 V maximum voltage.

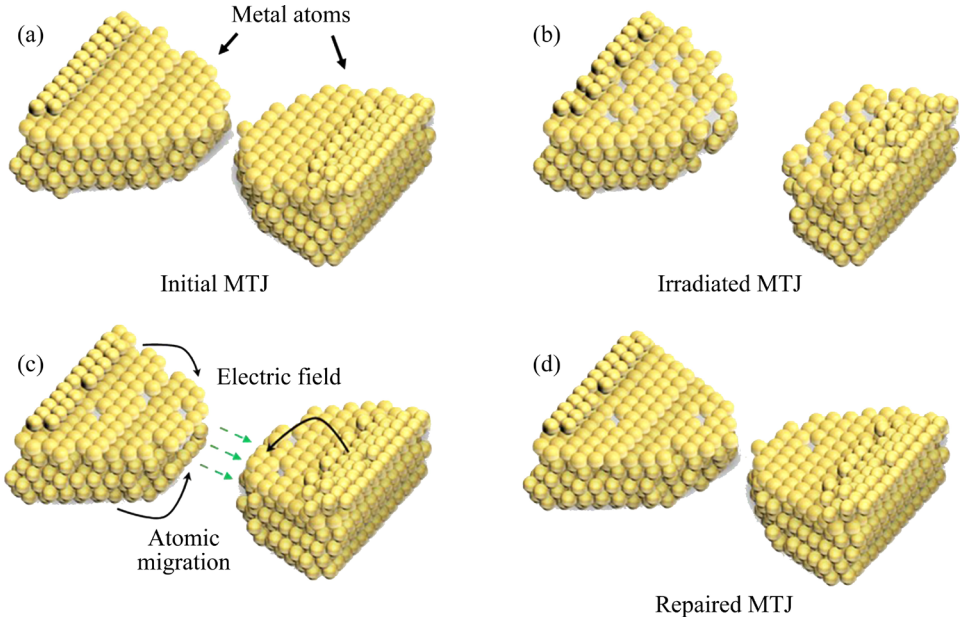

Fig. 5 Illustration of repairing process of irradiated MTJ devices: (a, b) Electrode tips before and after irradiation, respectively; (c) Migration of metal atoms towards apexes during double *I*−*V* sweeps; (d) Repaired electrode tips

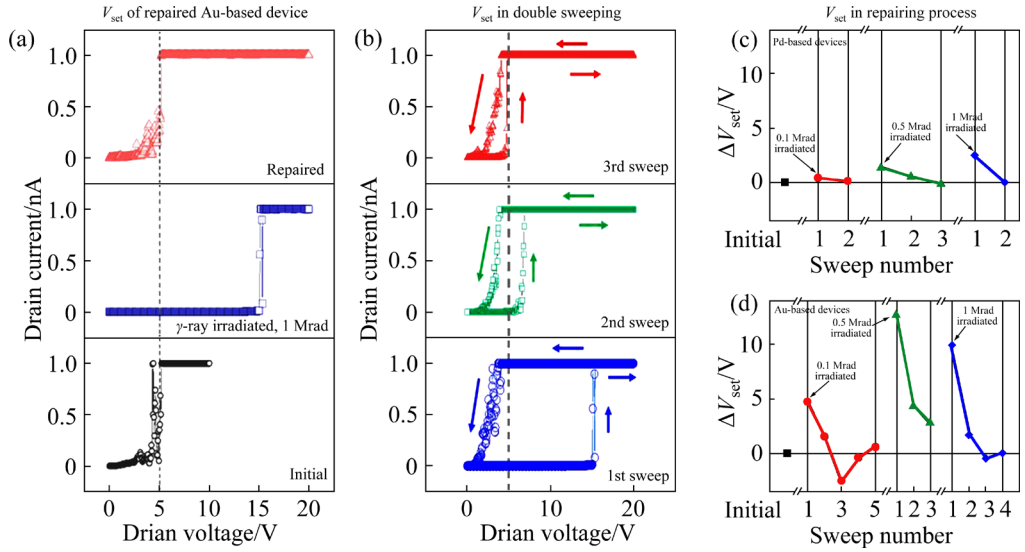

Fig. 6 Repairing process of irradiated Pd- and Au-based devices by configured double *I*−*V* sweeps: (a) Fully restored shift in V_{set} to its initial value; (b) Typical repairing process of Au-based devices by applying double *I*−*V* sweeps; (c, d) Change of ΔV_{set} in repairing process of Pd- and Au-based devices, respectively

The rising edges of the *I*−*V* curves shift left, showing a reduction in V_{set}, an increase in tunneling current, and a decrease in tunneling distance. The sweeps continue until the initial V_{set} is restored. Figures 6(c) and (d) show ΔV_{set} changes for typical Pd- and Au-based devices, respectively.

The number of double *I*−*V* sweeps required for repair depends on the magnitude of ΔV_{set}, and it is not strictly fixed. Pd-based devices usually need 1−3 sweeps, while Au-based devices may require up to 5 or more due to a larger ΔV_{set}. The repair process is similar for devices irradiated with either *β*- or *γ*-radiation, as shown in Fig. S6 in SM. Insufficient sweeps may lead to partial repair, with a larger remaining ΔV_{set}. For example, an Au-based device irradiated with 0.5 Mrad of *γ*-radiation and subjected to only 3 double sweeps showed a ΔV_{set} of 2.7 V after repair, indicating partial repair.

Notably, full repair of irradiated MTJ devices is achievable. With sufficient time and double *I*−*V* sweeps, ΔV_{set} can be reduced to be less than 0.2 V. This demonstrates that the impact of *γ*- and

β-radiation can be nearly eliminated through the repair process, which uses parameters with similar ranges to normal read operations. Thus, MTJ devices can be repaired with only on-chip circuits, without additional equipment or processes.

The in-situ repairability provided by MTJ devices offers significant potential in high γ- or β-radiation environments. Unlike conventional semiconductor devices, which require heavy shielding in normal operation and removal for annealing to repair radiation damage (often impossible in places like nuclear reactors or space missions), MTJs can be restored using on-chip circuits. The electrical parameters of repairing remain within the normal operational range, and the repair process is fast, taking seconds to several minutes. In memory arrays, radiation-induced errors in individual MTJ devices can be detected using checksum methods, and then data can be restored in-situ without affecting other devices. Without permanent damage, MTJ devices can withstand high-radiation environments for extended periods.

3.5 Generalized discussion on radiation resistivity in NOI structures

The radiation resistivity found in MTJ devices can be extended to other NOI devices like nanoscale vacuum tubes (NVT) and nanoscale air channel devices (NACD), which are of particular interest for their high switching speeds and potential use in future logic circuits. A study by FAN et al [29] explored the total ionizing dose (TID) and single event effect (SEE) of NACDs irradiated by X-ray and lasers. They found that NACD devices displayed strong radiation resistance, maintaining good gate control, high ON/OFF ratio, and large current density even after exposure to 1 Mrad of X-ray energy at 17 keV. Only a slight shift in the I−V curve was noted due to TID, suggesting that NACDs are radiation-immune and suitable for space applications.

The intrinsic radiation resistivity of NOI devices stems from both metals' immunity to radiolytic damage and the lack of a semiconductor channel or dielectric medium. We note that this radiation resistivity may vary depending on the device's conditions and design. In MTJ devices, the inherent radiation resistance is reflected as (1) immunity to permanent radiation damage; (2) continuing to operate normally despite radiation exposure; (3) repairability with in-situ conditions. On the other hand, NACD embodies the radiation resistance as their emission current is governed only by the electric field [57]. Without sensitive semiconductor channels or PN junctions, TID in NACDs causes only a slight shift in I−V curves due to accumulated charges in substrates, and parasitic thyristor effect is avoided in SEE.

In summary, the radiation immunity of NACD observed in Ref. [29] and the repairability of MTJ devices demonstrated in this work represent two typical forms of radiation resistivity inherent in NOI structures. This suggests that radiation resistivity may manifest in various forms across different NOI devices, depending on their designs and working conditions. Nevertheless, these manifestations can be analyzed using a similar framework as proposed in Section 3.4.

4 Conclusions

(1) Nanoscale MTJ devices were fabricated by electromigration method, and the impacts of γ- and β-radiation on their electrical properties were studied.

(2) After irradiation, the V_{set} of the MTJ device increases, with ΔV_{set} exhibiting a positive correlation with the doses in statistical analysis, albeit not strictly quantitatively. No significant relationship between the energy of electron beam with ΔV_{set} is observed. Au-based devices show larger ΔV_{set} compared to Pd-based devices at the same doses. No permanent or fatal damages are found to the devices, which are all functional normally after irradiation except for the change. Both γ- and β-radiation have similar impacts on the MTJ devices.

(3) Based on the theory of radiation damage on metal, it is inferred that the impacts stem from high-energy electrons excited by γ- and β-radiation. Radiation-induced random atomic displacement and migration, combined with the structure of electrode tips, created an unbalanced trend in the change of tunneling distance and tunneling current, resulting in an increase tunneling distance in most devices.

(4) MTJ devices demonstrate the capability for in-situ repair using carefully configured double I−V sweeps implemented with on-chip circuits. The repairability of irradiated MTJ devices is discussed as a form of radiation resistivity in NOI structures,

with potential generalization to other NOI devices such as NACD. These findings highlight the promising potential of MTJ devices for use in high-radiation environments, such as space stations, satellites, reactors, and synchrotron radiation sources.

CRediT authorship contribution statement

Zhong-zheng TIAN: Investigation, Data curation, Formal analysis, Visualization, Writing − Original manuscript preparation; **Da-cheng YU**, **Zhong-yang REN**, **Jiao-jiao TIAN** and **Li-ming REN:** Writing – Review & editing; **Yun-yi FU:** Funding acquisition, Supervision, Conceiving the project, Formal analysis, Writing – Editing & reviewing.

Declaration of competing interest

The authors declare that they have no known competing financial interests or personal relationships that could have appeared to influence the work reported in this paper.

Acknowledgments

This work was financially supported by the National Natural Science Foundation of China (Nos. T2293703, T2293700), and the Instrumental Analysis Fund of Peking University, China (No. KF-2305-07).

Supplementary Materials

Supplementary Materials in this paper can be found at: http://tnmsc.csu.edu.cn/download/19-p3836-2024-0331-Supplementary_Materials.pdf.

References

[1] DZHAFAROV T D, AKÇIZ C S, ÖREN D. Effect of electron irradiation on the photovoltaic characteristics of GaAs p−n junctions [J]. Thin Solid Films, 1998, 312(1/2): 327−330.

[2] TAYLOR D M, MEHDI Q H. Electron-beam-induced conduction in SiO_2 thin films [J]. Journal of Physics D: Applied Physics, 1979, 12(12): 2253−2267, 2262.

[3] MILGRAM ALVIN A. Ion-induced electrical breakdown in metal-oxide-silicon capacitors [J]. Journal of Applied Physics, 1990, 67(3): 1461−1470.

[4] AITKEN J M, YOUNG D R, PAN K. Electron trapping in electron-beam irradiated SiO_2 [J]. Journal of Applied Physics, 1978, 49(6): 3386−3391.

[5] SUÑÉ J, FARRÉS E, PLACENCIA I, BARNIOL N, MARTÍN F, AYMERICH X. Nondestructive multiple breakdown events in very thin SiO_2 films [J]. Applied Physics Letters, 1989, 55(2): 128−130.

[6] ZIOMEK W, MOSCICKA-GRZESIAK H. Relation of breakdown voltage and prebreakdown microdischarge parameters in vacuum [J]. IEEE Transactions on Electrical Insulation, 1993, 28(4): 481−487.

[7] NGUYEN D N, LEE C I, JOHNSTON A H. Total ionizing dose effects on flash memories [C]//IEEE Radiation Effects Data Workshop. New York, 1998: 100−103.

[8] DING Li-li, GNANI E, GERARDIN S, BAGATIN M, DRIUSSI F, PALESTRI P, SELMI L, LE ROYER C, PACCAGNELLA A. Total ionizing dose effects in Si-based tunnel FETs [J]. IEEE Transactions on Nuclear Science, 2014, 61(6): 2874−2880.

[9] FAN Lin-jie, BI Jin-shun, XI Kai, YAN Guang-ping. Investigation of radiation effects on FD-SOI hall sensors by TCAD simulations [J]. Sensors (Basel, Switzerland), 2020, 20(14): E3946.

[10] HARA K, KOCHIYAMA M, MOCHIZUKI A, SEGA T, ARAI Y, FUKUDA K, HAYASHI H, HIROSE M, IDA J, IKEDA H, IKEGAMI Y, IKEMOTO Y, ISHINO H, KAWAI Y, KOHRIKI T, KOMATSUBARA H, MIYAKE H, MIYOSHI T, OHNO M, OKIHARA M, TERADA S, TSUBOYAMA T, UNNO Y. Radiation resistance of SOI pixel devices fabricated with OKI 0.15 μm FD-SOI technology [J]. IEEE Transactions on Nuclear Science, 2009, 56(5): 2896−2904.

[11] SEMPLE J, WYATT-MOON G, GEORGIADOU D G, MCLACHLAN M A, ANTHOPOULOS T D. Semiconductor-free nonvolatile resistive switching memory devices based on metal nanogaps fabricated on flexible substrates via adhesion lithography [J]. IEEE Transactions on Electron Devices, 2017, 64(5): 1973−1980.

[12] SUGA H, SUZUKI H, SHINOMURA Y, KASHIWABARA S, TSUKAGOSHI K, SHIMIZU T, NAITOH Y. Highly stable, extremely high-temperature, nonvolatile memory based on resistance switching in polycrystalline Pt nanogaps [J]. Scientific Report, 2016, 6(1): 34961.

[13] TAKAHASHI T, FURUTA S, MASUDA Y, KUMARAGURUBARAN S, SUMIYA T, ONO M, HAYASHI Y, SHIMIZU T, SUGA H, HORIKAWA M, NAITOH Y. 4kb nonvolatile nanogap memory (NGpM) with 1 ns programming capability [C]//2012 IEEE Silicon Nanoelectronics Workshop (SNW). Honolulu, HI, USA, 2012: 1−2.

[14] NAITOH Y, HORIKAWA M, SUGA H, SHIMIZU T, FURUTA S, MASUDA Y, SUMIYA T, TAKAHASHI T, ONO M. Physical model of nonvolatile resistance switching using simple nanogap electrode [J]. ECS Meeting Abstracts, 2012, 2(37): 2849.

[15] TANG Zeng-min, ZHANG Ling, DU Jing-jing, XU Li-jian. Deposition of Pd on $Co(OH)_2$ nanoplates in stabilizer-free aqueous phase for catalytic reduction of 4-nitrophenol [J]. Transactions of Nonferrous Metals Society of China, 2022, 32(6): 1994−2002.

[16] LIU Xin-yi, WANG Ying-min, QIANG Jian-bing, WANG Bao-lin, MA Dian-guo, ZHANG Wei, DONG Chuang. Preparation and electro-catalytic activity of nanoporous palladium by dealloying rapidly-quenched $Al_{70}Pd_{17}Fe_{13}$ quasicrystalline alloy [J]. Transactions of Nonferrous Metals Society of China, 2019, 29(4): 785−790.

[17] SUGA H, SUZUKI H, OTSU K, ABE T, UMETA Y, TSUKAGOSHI K, SUMIYA T, SHIMA H, AKINAGA H,

NAITOH Y. Feedback electromigration assisted by alternative voltage operation for the fabrication of facet-edge nanogap electrodes [J]. ACS Applied Nano Materials, 2020, 3(5): 4077−4083.

[18] EGERTON R F. Control of radiation damage in the TEM [J]. Ultramicroscopy, 2013, 127: 100−108.

[19] EGERTON R F, LI P, MALAC M. Radiation damage in the TEM and SEM [J]. Micron, 2004, 35(6): 399−409.

[20] BAE D S, LEE S P, CHO Y R, TAKAHASHI H. Effect of aging treatment on irradiation-induced segregation of high Mn−Cr steel [J]. Transactions of Nonferrous Metals Society of China, 2011, 21(Suppl. 1): 58−61.

[21] LIU Man-ping, SUN Shao-chun, ROVEN HANS J, YU Ying-da, ZHANG Zhen, MURASHKIN M, VALIEV Z. Deformation defects and electron irradiation effect in nanostructured Al−Mg alloy processed by severe plastic deformation [J]. Transactions of Nonferrous Metals Society of China, 2012, 22(8): 1810−1816.

[22] LI Chang, WANG Hong-lei, YANG Ya-ping, GU Quan-chao, YAN Xing-heng, ZHOU Xin-gui. Blast and tensile properties of tantalum/niobium lined SiC/SiC composite tubes for nuclear cladding [J]. Transactions of Nonferrous Metals Society of China, 2022, 32(6): 1961−1968.

[23] LI Bin, FENG Yi, DING Ke-wang, QIAN Gang, ZHANG Xue-bin, LIU Yan-fang. Effect of electron beam irradiation on multi-walled carbon nanotubes [J]. Transactions of Nonferrous Metals Society of China, 2014, 24(3): 764−769.

[24] REN Ling, WANG Lin-jun, SU Qing-feng, LIU Jian-min, XU Run, PENG Hong-yan, SHI Wei-min, XIA Yi-ben. Annealing effect and irradiation properties of HFCVD diamond films [J]. Transactions of Nonferrous Metals Society of China, 2006, 16(Suppl.): 317−320.

[25] HAN J W, SEOL M L, MOON D I, HUNTER G, MEYYAPPAN M. Nanoscale vacuum channel transistors fabricated on silicon carbide wafers [J]. Nature Electronics, 2019, 2(9): 405−411.

[26] NIRANTAR S, AHMED T, REN Guang-hui, GUTRUF P, XU Cheng-long, BHASKARAN M, WALIA S, SRIRAM S. Metal–air transistors: semiconductor-free field-emission air-channel nanoelectronics[J]. Nano Letters, 2018, 18(12): 7478−7484.

[27] RAVARIU C. Vacuum nano-triode in nothing-on-insulator configuration working in terahertz domain [J]. IEEE Journal of the Electron Devices Society, 2018, 6: 1115−1123.

[28] SRISONPHAN S, JUNG Y S, KIM H K. Metal–oxide–semiconductor field-effect transistor with a vacuum channel [J]. Nature Nanotechnology, 2012, 7(8): 504−508.

[29] FAN Lin-jie, ZHAO Bi-yao, CHEN Bai-hong, MA Yue, BI Jin-shun, ZHAO Fa-zhan. Radiation immune-planar two-terminal nanoscale air channel devices toward space applications [J]. ACS Applied Nano Materials, 2023, 6(23): 22080−22087.

[30] MASUDA Y, TAKAHASHI T, FURUTA S, ONO M, SHIMIZU T, NAITOH Y. Control of nanogap junction resistance by imposed pulse voltage [J]. Applied Surface Science, 2009, 256(4): 1028−1030.

[31] FURUTA S, TAKAHASHI T, NAITOH Y, HORIKAWA M, SHIMIZU T, ONO M. Dependence of electric properties of a nanogap junction on electrode material [J]. Japanese Journal of Applied Physics, 2008, 47(3): 1806−1812.

[32] NAITOH Y, HORIKAWA M, ABE H, SHIMIZU T. Resistance switch employing a simple metal nanogap junction [J]. Nanotechnology, 2006, 17(22): 5669−5674.

[33] HIROSHI S, TOURU S, MASAYO H. Threshold current density of the resistance switching in Pt nanogap electrode [J]. Japanese Journal of Applied Physics, 2011, 50(6S): 06GF11.

[34] TODOROV T N, HOEKSTRA J, SUTTON A P. Current-induced forces in atomic-scale conductors [J]. Philosophical Magazine B, 2000, 80(3): 421−455.

[35] SORBELLO R S. Theory of the direct force in electro-migration [J]. Physical Review B, 1985, 31(2): 798−804.

[36] RICE-EVANS P, AUNG Z. On the decay of cobalt 60 [J]. The European Physical Journal A: Hadrons and Nuclei, 1970, 240(5): 392−395.

[37] KRASNOV A A, LEGOTIN S A, MURASHEV V N, DIDENKO S I, RABINOVICH O I, YURCHUK S Y, OMELCHENKO Y K, YAKIMOV E B, STARKOV V. Development and investigation of silicon converter beta radiation ^{63}Ni isotope [J]. IOP Conference Series of Materials Science and Engineering, 2016, 110(1): 012029.

[38] POLIKARPOV M A, YAKIMOV E B. Characterization of Si convertors of beta-radiation in the scanning electron microscope [J]. Solid State Phenomena, 2015, 242: 312−315.

[39] BROSI A R, BORKOWSKI C J, CONN E E, GRIESSY J C Jr. Characteristics of Ni^{59} and Ni^{63} [J]. Physical Review, 1951, 81(3): 391−395.

[40] LU Y, LI S L, AN J, LIU Y B. Surface modification of Al−Pb alloy by high current pulsed electron beam [J]. Transactions of Nonferrous Metals Society of China, 2006, 16(Suppl.): 14−19.

[41] TAO H Z, DONG G P, XIAO H Y, LIN C G, ZHAO X J. Second-order nonlinear optical properties of Ge−Ga−Ag−S glass irradiated by electron beam [J]. Transactions of Nonferrous Metals Society of China, 2006, 16(Suppl.): 170−173.

[42] SUGA H, HORIKAWA M, ODAKA S, MIYAZAKI H, TSUKAGOSHI K, SHIMIZU T, NAITOH Y. Influence of electrode size on resistance switching effect in nanogap junctions [J]. Applied Physics Letters, 2010, 97(7): 073118.

[43] DING Man, CHENG Yong-hong, LIU Xin, LI Xiao-long. Total dose response of hafnium oxide based metal−oxide−semiconductor structure under gamma-ray irradiation [J]. IEEE Transactions on Dielectrics and Electrical Insulation, 2014, 21(4): 1792−1800.

[44] FRIEDLAND E. Radiation damage in metals [J]. Critical Reviews in Solid State and Materials Sciences, 2001, 26(2): 87−143.

[45] BRINKMAN J A. On the nature of radiation damage in metals [J]. Journal of Applied Physics, 1954, 25(8): 961−970.

[46] NORDLUND K, ZINKLE S J, SAND A E, GRANBERG F, AVERBACK R S, STOLLER R E, SUZUDO T, MALERBA L, BANHART F, WEBER W, WILLAIME F, DUDAREV S L, SIMEONE D. Primary radiation damage: A review of current understanding and models [J]. Journal of Nuclear Materials, 2018, 512: 450−479.

[47] KWON J, MOTTA A T. Gamma displacement cross-sections in various materials [J]. Annals of Nuclear Energy, 2000, 27(18): 1627−1642.
[48] GLEN J W. A survey of irradiation effects in metals [J]. Advances in Physics, 1955, 4(16): 381−477.
[49] NELSON G, REWY D. Passive nondestructive analysis of nuclear materials [M]. Los Alamos: Los Alamos National Laboratory, 1991: 27−42.
[50] LIN Ying-hong. A study of the secondary electrons [D]. Knoxville: University of Tennessee, 2007: 21−47.
[51] CAMPBELL B, MAINWOOD A. Radiation damage of diamond by electron and gamma irradiation [J]. Physica Status Solidi (a): Applied Research, 2000, 181(1): 99−107.
[52] GLYDE H R. Relation of vacancy formation and migration energies to the Debye temperature in solids [J]. Journal of Physics and Chemistry of Solids, 1967, 28(10): 2061−2065.
[53] SORBELLO R S. Recoil-enhanced atomic migration [J]. Physical Review Letters, 1989, 63(17): 1815−1818.
[54] GU Heng-fei, LI Ge-ping, LIU Cheng-ze, YUAN Fu-sen, HAN Fu-zhou, ZHANG Li-feng, WU Song-quan. Considerable knock-on displacement of metal atoms under a low energy electron beam [J]. Scientific Reports, 2017, 7(1): 184.
[55] KITTIRATANAWASIN L, SMITH R, UBERUAGA B P, SICKAFUS K. Displacement threshold and Frenkel pair formation energy in ionic systems [J]. Nuclear Instruments and Methods in Physics Research, 2010, 268(19): 2901−2906.
[56] BEN-ABRAHAM S I, RABINOVITCH A, PELLEG J. Relations between vacancy migration and formation energies, Debye temperature and melting point [J]. Physica Status Solidi (b), 1977, 84(2): 435−441.
[57] SIMMONS J G. Generalized formula for the electric tunnel effect between similar electrodes separated by a thin insulating film [J]. Journal of Applied Physics, 1963, 34(6): 1793−1803.
[58] LIDE D R. CRC handbook of chemistry and physics [M]. 85th ed. New York: CRC Press, 2004: 12−124.
[59] HASHIZUMEI T, KAMIYA I, HASEGAWA Y, SANO N, SAKURAI T, PICKERING H W. A role of a tip geometry on STM images [J]. Journal of Microscopy, 1988, 152(2): 347−354.
[60] PETHICA J B, OLIVER W C. Tip surface interactions in STM and AFM [J]. Physica Scripta, 1987, T19: 61−66.
[61] TSONG T T. Effects of an electric field in atomic manipulations [J]. Physical Review B, 1991, 44(24): 13703−13710.

γ 和 β 辐射对金属隧穿结器件的影响及其可修复性

田仲政，于达程，任中阳，田姣姣，任黎明，傅云义

北京大学 集成电路学院，北京 100871

摘　要：通过电迁移方法制备了纳米尺度的金属隧穿结(MTJ)器件，并研究了 γ 和 β 辐射对其电学性能的影响。辐照后，MTJ 器件的 SET 电压(V_{set})增加，器件从低阻态(LRS)转换为高阻态(HRS)。γ 和 β 射线辐照激发出高能电子，高能电子引起原子位移，导致 SET 电压的漂移。但是，与半导体器件不同，辐照不会对 MTJ 器件造成永久性或致命损伤。MTJ 器件可以在原位或片上条件下，通过多次双向 I–V (I 为电流；V 为电压)扫描方法，使器件恢复至辐照前的状态。这表明 MTJ 器件在辐照环境下具有良好的应用潜力。MTJ 器件在辐照后的可修复性与其 nothing-on-insulator (NOI)结构密切相关，这一特性也可推广至其他 NOI 器件或金属基微米/纳米器件中。

关键词：γ 辐照；β 辐照；纳米间隙；金属隧穿结；辐照损伤

(Edited by Wei-ping CHEN)